Inductance Dual Model and Control of Multiphase Coupled Inductor Buck Converter

Daniel Zhou†, Youssef Elasser†, Jaeil Baek†, Charles R. Sullivan‡, and Minjie Chen†
†*Princeton University, Princeton NJ, United States*
‡*Dartmouth College, Hanover NH, United States*
Email: {dz8, minjie}@princeton.edu

***Abstract*—This paper presents an inductance dual model for designing coupled inductors in multiphase buck converters. The model is derived as a topological dual of the reluctance model of a multiphase coupled inductor, yielding an inductance-based equivalent circuit with simplified equations for evaluating the transient and steady state performance. The model clearly relates the magnetic geometry to a lumped circuit model, allowing visualization of coupling relationships and magnetic flux in SPICE. The model is conducive to state space and transfer function analysis. The dynamic equations of the M-phase coupled inductor buck converter are derived. It is revealed that the duty ratio to output voltage transfer function of a multiphase coupled inductor buck converter is equivalent to that of a single-phase buck converter. The inductance dual is leveraged to design a programmable coupled inductor that modulates the center leg reluctance to improve the control bandwidth.**

***Index Terms*—inductance dual model, state space model, transfer function, coupled inductor, multiphase buck converter.**

I. Introduction

A FUNDAMENTAL challenge of designing multiphase buck converters for point-of-load applications is to balance the steady state voltage ripple and transient response requirements [1]. A larger discrete inductance reduces steady state ripple at the cost of incurring a slower transient response. By using coupled inductors with cross-coupled switching, one can reduce the current ripple while maintaining fast transient performance. Moreover, magnetic core size and output capacitor size can be reduced.

Traditionally, the coupled inductor in a multiphase buck converter is modeled based on the inductance matrix, a reluctance circuit model, or a multiphase coupled transformer model [2]–[10]. However, the inductance matrix methods often lead to long and unwieldy design equations; the reluctance circuit model is cumbersome to simulate, and the multiphase coupled transformer model cannot provide a straightforward link between magnetic structure and circuit design.

This paper investigates an inductance dual model for multiphase coupled inductors as a topological dual of a traditional reluctance circuit model. The inductance dual model directly links the coupled inductor geometry to the lumped circuit model by way of magnetic reluctance. Simple equations for effective inductance and current ripple are derived which provide useful insights to magnetic design. The inductance dual model is suitable for visualization of flux in sophisticated coupling relationships using SPICE.

The modelling methods for classical buck converters are well understood [11]. Multiphase coupled inductor buck circuits have been studied [12], [13], but these dynamic models are typically restricted to two phases and are not easily extensible to an arbitrary number of phases M. We leverage the inductance dual model to derive the state space model and transfer function of an M-phase coupled inductor buck converter. The control equations are expressed in terms of magnetic reluctance, simultaneously simplifying them and elucidating the impact of physical core design on dynamic properties. Moreover, the model reveals that the duty ratio to output voltage transfer function of a symmetric multiphase coupled inductor buck converter is a second order system identical to a single phase buck, with parameters only related to the leakage inductance but not the magnetizing inductance.

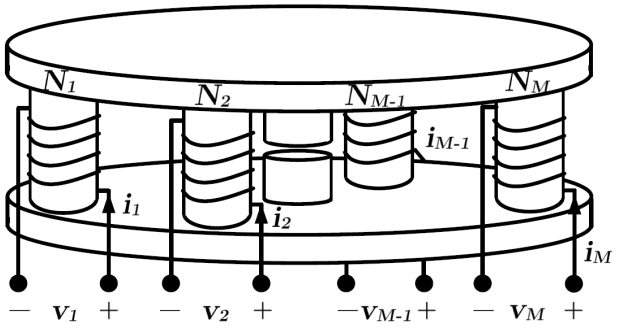

Fig. 1. Multiphase coupled magnetics with many symmetric windings. This structure has $M = 4$ side legs and a center leg with an air gap.

II. Principles of the Inductance Dual Model

Fig. 1 shows a multiphase coupled inductor with $M = 4$ side legs and one shared center leg. Each winding with N turns is coupled to one leg of the core and the center leg with reluctance $\mathcal{R}_C$ provides a return path for flux. Fig. 2a shows a reluctance model of the magnetic core structure for an arbitrary number of phases. Fig. 2b shows the inductance dual model. The reluctance and inductance dual models are topological duals. To simplify the following analysis and derivation, the reluctance of the top and bottom plates are neglected. All windings are assumed to have the same number of turns N, and all legs have identical reluctance $\mathcal{R}_L$. However, the reluctance and inductance dual models can be extended to describe asymmetric coupling and arbitrary N.

The inductance dual model is a lumped circuit model with inductors and ideal transformers that can be directly used

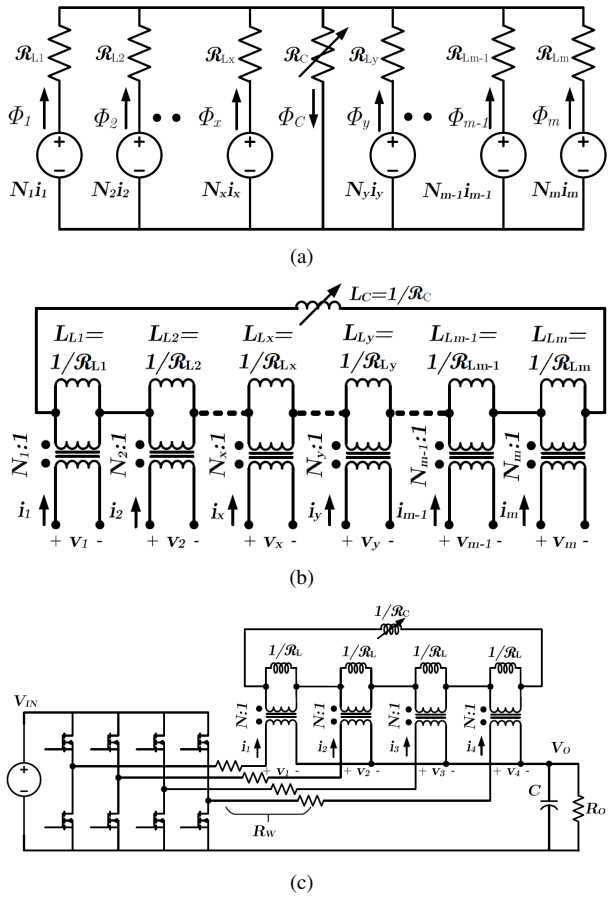

Fig. 2. (a) Reluctance circuit model and (b) inductance dual model of a multiphase coupled inductor with M windings. The reluctance of the x^{th} leg is $\mathcal{R}_{Lx}$, and the reluctance of the center leg is $\mathcal{R}_C$. (c) Four phase buck converter with coupled inductor modelled using the inductance dual model. The center leg reluctance $\mathcal{R}_C$ may or may not be adjustable.

in SPICE simulations [14], [15]. The current through the inductors in the topological dual is is proportional to flux in the corresponding core leg. [16], [17]. Therefore, the flux and voltage in each winding can be simply extracted and used in existing core loss models, which commonly use Steinmetz's equation or its extensions [18]–[20]. The inductance dual model also has the advantage of avoiding any "invisible" coupling between inductors: the lumped circuit model naturally describes all coupling relationships. In SPICE simulations, the ideal transformers in the inductance dual model must work in DC to model the DC flux in the magnetic core.

The inductance dual model in Fig. 2b leads to a reluctance matrix $\mathcal{R}_{M\times M}$ which describes the relationship between the derivative of the current in the M windings and the voltage drop across the M windings:

$$\begin{bmatrix} \frac{di_1}{dt} \\ \frac{di_2}{dt} \\ \vdots \\ \frac{di_M}{dt} \end{bmatrix} = \overbrace{\frac{1}{N^2}\begin{bmatrix} \mathcal{R}_L+\mathcal{R}_C & \mathcal{R}_C & \cdots & \mathcal{R}_C \\ \mathcal{R}_C & \mathcal{R}_L+\mathcal{R}_C & \cdots & \mathcal{R}_C \\ \vdots & \vdots & \ddots & \vdots \\ \mathcal{R}_C & \mathcal{R}_C & \cdots & \mathcal{R}_L+\mathcal{R}_C \end{bmatrix}}^{\mathcal{R}_{M\times M}} \begin{bmatrix} v_1 \\ v_2 \\ \vdots \\ v_M \end{bmatrix}. \tag{1}$$

Traditional methods for modelling coupled inductors typically use an inductance matrix parameterized by the self inductance

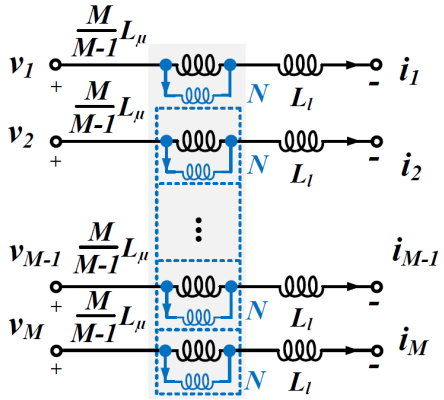

Fig. 3. Multiwinding transformer model of the structure in Fig. 1 implemented with an ideal current equalizing transformer (blue), and magnetizing and leakage inductances. The ideal current equalizing transformer equalizes the $\mathcal{MMF}$ of all windings and forces the sum of the volts-per-turn to be zero.

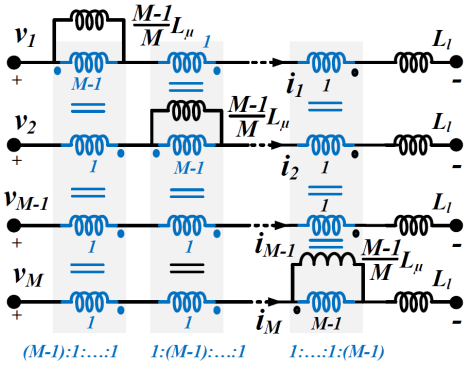

Fig. 4. Multiwinding transformer model of the structure in Fig. 1 implemented with $M-1$ voltage equalizing transformers. Each ideal voltage equalizing transformer equalizes the volt-per-turn of all windings and forces the sum of $\mathcal{MMF}$ of all windings to be the zero.

L_S and mutual inductance L_M:

$$\begin{bmatrix} v_1 \\ v_2 \\ \vdots \\ v_M \end{bmatrix} = \begin{bmatrix} L_S & L_M & \cdots & L_M \\ L_M & L_S & \cdots & L_M \\ \vdots & \vdots & \ddots & \vdots \\ L_M & L_M & \cdots & L_S \end{bmatrix} \begin{bmatrix} \frac{di_1}{dt} \\ \frac{di_2}{dt} \\ \vdots \\ \frac{di_M}{dt} \end{bmatrix}. \tag{2}$$

If $\mathcal{R}_C$ and $\mathcal{R}_L$ are positive scalars, which is the case in practice, $\mathcal{R}_{M\times M}$ is invertible. It may be shown by matching the elements of (2) with ${\mathcal{R}_{M\times M}}^{-1}$ that L_M and L_S are

$$L_S = \frac{N^2}{\mathcal{R}_L + \frac{\mathcal{R}_L}{M-1}||\mathcal{R}_C} = \frac{N^2(\mathcal{R}_L+(M-1)\mathcal{R}_C)}{\mathcal{R}_L(\mathcal{R}_L+M\mathcal{R}_C)},$$

$$L_M = \frac{-N^2(\frac{\mathcal{R}_L}{M-2}||\mathcal{R}_C)}{(\mathcal{R}_L+\frac{\mathcal{R}_L}{M-1}||\mathcal{R}_C)(\mathcal{R}_L+\frac{\mathcal{R}_L}{M-2}||\mathcal{R}_C)} = \frac{-N^2\mathcal{R}_C}{\mathcal{R}_L^2+M\mathcal{R}_L\mathcal{R}_C}, \tag{3}$$

which can also be found from the definition of self and mutual inductance and Fig. 2. Note L_M is negative, indicating that the phases are negatively coupled. The inductance dual circuit model is interchangeable with $\mathcal{R}_{M\times M}$, L_S, and L_M.

The inductance dual model is also interchangeable with other models. Figure 3 shows one example implementation of the multiwinding transformer model by using an ideal current equalizing transformer [4], [5]. The magnetizing inductance of

each winding is $\frac{M}{M-1}L_\mu$ and the leakage inductance of each winding is L_l. An inductance matrix describes the multiwinding transformer model mathematically. The self inductance of of this model is $L_\mu + L_l$. The mutual inductance of this model is $-\frac{1}{M-1}L_\mu$. The turns ratio of the multiwinding transformer is $\{N : N : ... : N\}$. Figure 4 shows another example implementation of the multiwinding transformer model by using an ideal voltage equalizing transformer model [8]. This model comprises M ideal voltage equalizing transformers with a turns ratio of $\{(M-1) : 1 : ... : 1\}$ (assuming all windings have equal number of turns). The magnetizing inductance reflected on the $\{M-1\}$ turn side is $\frac{M-1}{M}L_\mu$.

Similarly, L_l and L_μ are functions of $\mathcal{R}_L$ and $\mathcal{R}_C$ in the inductance dual model, as well as L_S and L_M in the inductance matrix model:

$$L_l = \frac{N^2}{\mathcal{R}_L + M\mathcal{R}_C} = L_S + (M-1)L_M, \tag{4}$$

$$L_\mu = \frac{N^2(M-1)\mathcal{R}_C}{\mathcal{R}_L(\mathcal{R}_L + M\mathcal{R}_C)} = -(M-1)L_M. \tag{5}$$

The inductance dual model is conducive to core design since it is is based on reluctances $\mathcal{R}_L$ and $\mathcal{R}_C$. The L_μ and L_l based multiwinding transformer model provides insights to controller design. Section IV reveals that the duty ratio to output voltage transfer function of an M-phase N-winding buck converter with a coupled inductor with center leg reluctance $\mathcal{R}_C$ and side leg reluctance $\mathcal{R}_L$, is equivalent to an M-phase uncoupled buck converter with a per-phase inductance of $L_l = \frac{N^2}{\mathcal{R}_L + M\mathcal{R}_C}$ or a single phase buck with inductance L_l/M.

III. Multiphase Coupled Inductor Buck Design

Coupled inductors can enhance the performance of multiphase buck converters. By coupling the multiple inductors with a high permeability magnetic core, one can reduce the current ripple in each phase and also reduce the conduction loss in switches, windings, and traces. Many methods have been developed to evaluate the performance of a coupled inductor design in multiphase buck converters . Based on the inductance matrix model, [3] predicts that the per-phase current ripple ratio between uncoupled and coupled cases if the transient inductances are the same for a two phase buck converter is:

$$\frac{\Delta i_{cp}}{\Delta i_{noncp}} = \frac{1 + \frac{D}{1-D}\alpha}{1-\alpha}. \tag{6}$$

Here $\alpha = \frac{L_M}{L_S} = -\frac{\mathcal{R}_C}{\mathcal{R}_L + \mathcal{R}_C}$. D is the duty ratio. This ripple ratio is an important figure-of-merit ($\mathcal{FOM}$) for evaluating coupled inductor design. A smaller ripple ratio is better. Substituting α into (6), the ripple ratio becomes a function of $\mathcal{R}_L$, $\mathcal{R}_C$, and duty ratio D:

$$\frac{\Delta i_{cp}}{\Delta i_{noncp}} = \frac{(1-D)\mathcal{R}_L + (1-2D)\mathcal{R}_C}{(1-D)(\mathcal{R}_L + 2\mathcal{R}_C)}. \tag{7}$$

This equation was generalized in [19] for a M-phase coupled inductor buck converter with $0 < D < \frac{1}{M}$ by using a multiwinding transformer model. Defining ρ as the ratio between L_μ and L_l in the multiwinding transformer model (Fig. 4):

$$\rho = \frac{L_\mu}{L_l} = \frac{(M-1)\mathcal{R}_C}{\mathcal{R}_L}. \tag{8}$$

The ripple ratio is a function of M, D, $\mathcal{R}_L$ and $\mathcal{R}_C$:

$$\frac{\Delta i_{cp}}{\Delta i_{noncp}} = \frac{\frac{M-1+\rho}{M-1+M\rho} - D}{1-D} = \frac{(1-D)\mathcal{R}_L + (1-MD)\mathcal{R}_C}{(1-D)(\mathcal{R}_L + M\mathcal{R}_C)}. \tag{9}$$

Four design parameters were defined in [8] based on the inductance matrix model for a M-phase coupled inductor buck converter with $\frac{k}{M} < D < \frac{k+1}{M}$, where $k = 0, .., (M-1)$ is the number of phases overlapping with the current phase.

1) Overall steady-state inductance (L_{oss}): the multiphase coupled inductor has the same total output peak-to-peak current ripple amplitude as a single discrete inductor with inductance L_{oss};
2) Per-phase steady-state inductance (L_{pss}): each phase of the multiphase coupled inductor has the same per-phase peak-to-peak current ripple amplitude as a single discrete inductor with inductance L_{pss};
3) Overall transient inductance (L_{otr}): the multiphase coupled inductor behaves as a single discrete inductor with inductance L_{otr} for the purposes of the overall transient performance and small signal model;
4) Per-phase transient inductance (L_{ptr}): the same as the overall transient inductance, but normalized on a per-phase basis.

These parameters are expressed as functions of L_S, L_M, D, M, and k in [8] based on the inductance matrix model:

$$\begin{aligned}
L_{oss} &= \frac{(1-D)DM(L_S + L_M(M-1))}{(DM-k)(1+k-DM)}, \\
L_{pss} &= \frac{(L_S - L_M)(L_S + (M-1)L_M)}{L_S + \left((M-2k-2) + \frac{k(k+1)}{MD} + \frac{MD(M-2k-1)+k(k+1)}{M(1-D)}\right)L_M}, \\
L_{otr} &= \frac{L_S + (M-1)L_M}{M}, \\
L_{ptr} &= L_S + (M-1)L_M.
\end{aligned} \tag{10}$$

The steady-state output current ripple, the output small-signal model, per-phase current ripple, and per-phase small-signal model of the multiphase coupled inductor in continuous-conduction-mode can be rapidly estimated. They are valid when operating the converter as a single phase buck converter with the same duty ratio D, the same switching frequency, and these effective inductance values.

Using (3), L_{pss}, L_{ptr}, L_{oss}, and L_{otr} can be expressed as functions of $\mathcal{R}_L$, $\mathcal{R}_C$, D, M, and k:

$$\begin{aligned}
L_{oss} &= \underbrace{\frac{(1-D)DM}{(k+1-DM)(DM-k)}}_{1/\delta} \times \underbrace{\frac{N^2}{\mathcal{R}_L + M\mathcal{R}_C}}_{L_{ptr}}, \\
L_{pss} &= \frac{N^2(1-D)}{-\frac{k^2\mathcal{R}_C}{DM} - \frac{k\mathcal{R}_C}{DM} + 2k\mathcal{R}_C - DM\mathcal{R}_C + \mathcal{R}_C - D\mathcal{R}_L + \mathcal{R}_L}, \\
L_{otr} &= \frac{1}{M} \times \underbrace{\frac{N^2}{\mathcal{R}_L + M\mathcal{R}_C}}_{L_{ptr}}, \\
L_{ptr} &= \frac{N^2}{\mathcal{R}_L + M\mathcal{R}_C} = L_l.
\end{aligned} \tag{11}$$

The per-phase transient inductance L_{ptr}, which is equal to the leakage inductance L_l in the multiwinding transformer model, is a key parameter in the design process. It is linearly

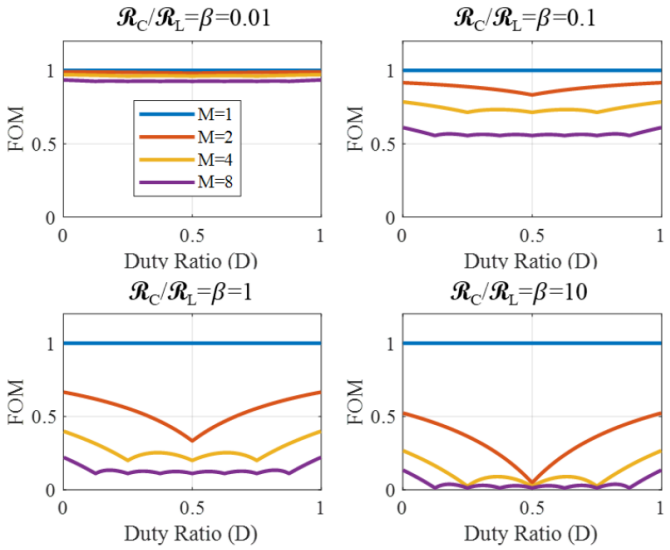

Fig. 5. $\mathcal{FOM}$ of the multiphase coupled buck inductor as functions of the number of phases (M), duty ratio (D), and reluctance ratio ($\beta = \mathcal{R}_C/\mathcal{R}_L$). A lower $\mathcal{FOM}$ indicates more winding current ripple reduction. A high β indicates strong coupling, and a low β indicates weak coupling.

related to the overall steady-state inductance L_{oss} by an interleaving factor $1/\delta$. $1/\delta$ quantifies the ripple reduction ratio if M discrete inductors are operated in interleaving [21], [22]. The overall transient inductance L_{otr} is linearly related to L_{ptr} by a factor $1/M$. Only L_{pss} is not proportional to L_{ptr}. For a given volumetric constraint on the coupled inductor, the first step is to select L_{ptr} based on the required L_{oss} and L_{otr}. Then, minimize the ratio between $\mathcal{R}_L$ and $\mathcal{R}_C$ to maximize L_{pss}. By explicitly including $\mathcal{R}_L$ and $\mathcal{R}_C$, (11) offers better geometric design insights than (10). A good strategy to design coupled inductors for multiphase buck converter is:

1) Selected a magnetic structure with $\mathcal{R}_L \ll \mathcal{R}_C$;
2) Choose an appropriate per-phase transient inductance (L_{ptr}) based on the overall transient requirements (L_{otr}), and the overall output ripple requirements (L_{oss}).
3) Determine $\mathcal{R}_L + M\mathcal{R}_C$ based on the selected L_{ptr}.
4) Design the magnetic structure (material and geometry) to minimize $\mathcal{R}_L$, maximize $\mathcal{R}_C$, optimize the loss, and ensure enough margin to avoid saturation.

We use the equations derived based on the inductance dual model to define a figure-of-merit ($\mathcal{FOM}$) for better understanding of the system. We define $\mathcal{FOM}$ as the ratio between the transient and steady-state inductance per-phase:

$$\begin{aligned}\mathcal{FOM} &= \frac{L_{ptr}}{L_{pss}} = \frac{\Delta i_{cp}}{\Delta i_{noncp}} \\ &= \frac{-\frac{k^2\mathcal{R}_C}{DM} - \frac{k\mathcal{R}_C}{DM} + 2k\mathcal{R}_C - DM\mathcal{R}_C + \mathcal{R}_C - D\mathcal{R}_L + \mathcal{R}_L}{(1-D)(\mathcal{R}_L + M\mathcal{R}_C)} \\ &= \frac{-\frac{k^2\beta}{DM} - \frac{k\beta}{DM} + 2k\beta - DM\beta + \beta - D + 1}{(1-D)(1+M\beta)}.\end{aligned} \tag{12}$$

Here $\beta = \frac{\mathcal{R}_C}{\mathcal{R}_L}$. This ratio $\mathcal{FOM}$ equals to the per-phase current ripple ratio $\frac{\Delta i_{cp}}{\Delta i_{noncp}}$. Figure 5 plots the $\mathcal{FOM}$s of a range of D, M, and β. $\mathcal{FOM}$ is always between zero and one. A smaller $\mathcal{FOM}$ is better. If $\beta \to +\infty$, $\mathcal{R}_C \gg \mathcal{R}_L$, the inductors are strongly coupled, the benefits of coupling increase. If $\beta \to 0$, $\mathcal{R}_L \ll \mathcal{R}_C$, the inductors are weakly coupled. Consequently, $\mathcal{FOM} \to 1$, and the benefits of coupling decrease. A software tool (*coupL*) for calculating these parameters is available at: http://www.princeton.edu/powerlab/coupL/coupL.html.

There are two ways of increasing β for a given $\{\mathcal{R}_L + M\mathcal{R}_C\}$ (which is directly related to L_{ptr}): 1) reducing $\mathcal{R}_L$; 2) increasing $\mathcal{R}_C$. However, $\mathcal{R}_C$ cannot be increased significantly while retaining the chosen value of L_{ptr}, so increasing β requires decreasing $\mathcal{R}_L$, which can be achieved by using high permeability core material, reducing the effective length, or extending the core area. Tradeoffs exist between core loss, saturation margin, energy storage requirements, and transient response. In an optimal design, the core loss, winding loss, efficiency, power density, and transient and steady-state performance are highly related and need to be jointly optimized for a given design specification.

In practical designs, there is always parasitic inductance adding to the leakage inductance L_l of the coupled inductor (Fig. 3 and Fig. 4) of the multiwinding transformer model. As L_l increases, the benefits of coupling diminish. Therefore, one should design the L_l of the coupled inductor resulting from the center leg and additional leakage inductance from other sources such as traces and connectors such that their combination achieves the desired transient performance.

The absolute value of the current ripple per-phase impacts the loss in the windings and switches. It is another key design parameter to be minimized:

$$\Delta i_{phase} = \frac{V_{IN}DT}{N^2}\left(-\frac{k^2\mathcal{R}_C}{DM} - \frac{k\mathcal{R}_C}{DM} + 2k\mathcal{R}_C - DM\mathcal{R}_C + \mathcal{R}_C - D\mathcal{R}_L + \mathcal{R}_L\right). \tag{13}$$

When $D = 0.5$, $M = 1$, $k = 0$, the effective inductance is $L_{pss} = \frac{N^2}{\mathcal{R}_C + \mathcal{R}_L}$, leading to the worst case inductor current ripple per-phase:

$$\Delta i_{max} = \frac{V_{IN}T(\mathcal{R}_C + \mathcal{R}_L)}{4N^2}. \tag{14}$$

IV. State Space Model of the Multiphase Coupled Inductor Buck Converter

The inductance dual model naturally leads to the derivation of a state space model for the multiphase coupled inductor buck converter and its associated transfer functions for an arbitrary number of phases M. In the following subsections, we develop the state-space model (IV-A), and use this model to find the transfer function (IV-B). The result is the same transfer function that of as a single-phase buck converter, a result that is also derived directly from circuit models in subsection IV-C. To simplify the derivations, we restrict our discussion to symmetric designs (identical reluctance $\mathcal{R}_L$, winding resistance R_w, number of turns N for each phase) without phase overlapping ($D < 1/M$). This analysis can be further extended to cover a generalized case with arbitrary D and phase overlapping.

A. State Space Model of the M-phase Converter

There are M inductors with independent currents and one capacitor in the system. As a result, there are $M + 1$ state

variables, yielding a state vector $\mathbf{x} = [i_1, i_2, \cdots, i_M, v_o]^T$. An M-phase coupled inductor buck converter has M sub-periods, each of duration $\frac{T}{M}$. In the k^{th} sub-period, one phase #k is connected to V_{IN} for a time DT, where $k = 1, ..., M$ and D is the duty cycle. (1) leads to the dynamic equation of each phase current. For example, for phase #1:

$$\begin{aligned} N^2 \frac{di_1}{dt} &= (\mathcal{R}_L + \mathcal{R}_C)v_1 + \mathcal{R}_C v_2 + \cdots + \mathcal{R}_C v_M \\ &= (\mathcal{R}_L + \mathcal{R}_C)v_1 + \mathcal{R}_C \sum_{j=2}^{j=M} v_j. \end{aligned} \tag{15}$$

Without phase overlapping, $D < 1/M$. If a phase #k is connected to V_{IN}, $v_k = V_{IN} - i_k R_w - v_o$, as shown in Fig. 2c. Otherwise, $v_k = -i_k R_w - v_o$. Taking phase #1 as connected to V_{IN} in (15), we obtain a dynamic equation in terms of state variables only.

$$\begin{aligned} N^2 \frac{di_1}{dt} &= (\mathcal{R}_L + \mathcal{R}_C)(V_{IN} - i_1 R_w - v_o) + \mathcal{R}_C \sum_{j=2}^{j=M} (-i_j R_w - v_o) \\ &= v_o(-\mathcal{R}_L - M\mathcal{R}_C) + i_1[-R_w(\mathcal{R}_L + \mathcal{R}_C)] - \mathcal{R}_C R_w \sum_{j=2}^{j=M} i_j \\ &\quad + V_{IN}(\mathcal{R}_L + \mathcal{R}_C). \end{aligned} \tag{16}$$

By changing indices, (16) can be extended to a general dynamic equation for any phase $k = 1, ..., M$, depending on whether that phase is the one that is connected to V_{IN}:

$$N^2 \frac{di_k}{dt} = \begin{cases} v_o(-M\mathcal{R}_C - \mathcal{R}_L) + i_k[-R_w(\mathcal{R}_C + \mathcal{R}_L)] - R_w\mathcal{R}_C \sum_{\substack{j=1 \\ j\neq k}}^{j=M} i_j \\ \quad + V_{IN}(\mathcal{R}_L + \mathcal{R}_C) \qquad \text{phase } k \text{ on} \\ v_o(-M\mathcal{R}_C - \mathcal{R}_L) + i_k[-R_w(\mathcal{R}_C + \mathcal{R}_L)] - R_w\mathcal{R}_C \sum_{\substack{j=1 \\ j\neq k}}^{j=M} i_j \\ \quad + V_{IN}(\mathcal{R}_C) \qquad \text{one phase on, not phase } k \end{cases}. \tag{17}$$

Next, the capacitor dynamic equation is obtained from the sum of all phase currents and the output current through a resistive load R_o:

$$\frac{dv_o}{dt} = \frac{1}{C} \sum_{j=1}^{j=M} i_j - \frac{v_o}{R_o C}. \tag{18}$$

Equations (17), (18), and the dynamic equations of the other phases are best represented in matrix form as a set of first-order differential equations. First, we define matrices A and $U^{(k)}$ as:

$$A = \frac{1}{N^2} \begin{bmatrix} -R_w(\mathcal{R}_C+\mathcal{R}_L) & -R_w\mathcal{R}_C & \cdots & -R_w\mathcal{R}_C & -M\mathcal{R}_C-\mathcal{R}_L \\ -R_w\mathcal{R}_C & -R_w(\mathcal{R}_C+\mathcal{R}_L) & \cdots & -R_w\mathcal{R}_C & -M\mathcal{R}_C-\mathcal{R}_L \\ \vdots & \vdots & \ddots & \vdots & \vdots \\ -R_w\mathcal{R}_C & -R_w\mathcal{R}_C & \cdots & -R_w(\mathcal{R}_C+\mathcal{R}_L) & -M\mathcal{R}_C-\mathcal{R}_L \\ N^2\frac{1}{C} & N^2\frac{1}{C} & \cdots & N^2\frac{1}{C} & -N^2\frac{1}{R_oC} \end{bmatrix}, \tag{19}$$

$$U^{(k)} = \frac{V_{IN}}{N^2} \begin{bmatrix} \mathcal{R}_C \\ \vdots \\ \mathcal{R}_C + \mathcal{R}_L \\ \vdots \\ \mathcal{R}_C \\ 0 \end{bmatrix} \begin{matrix} \text{row 1} \\ \\ \text{row k} \\ \\ \text{row M} \\ \text{row M+1.} \end{matrix}, \tag{20}$$

where we factor out the coefficient $\frac{1}{N^2}$ for legibility. Note that the $(M+1)\times(M+1)$ A matrix is always the same regardless of the phase connections. (20) is only valid when phase #k is connected to V_{IN} and all other phases are connected to ground; hence, we use a superscript (k). When no phase is connected to V_{IN}, the U matrix is zero.

To approximate the system dynamics over a full switching cycle, we average the equations of all switch states over a period T. This state space averaging technique, described in [11], is generally valid when the state $\mathbf{x}$ varies slowly compared to the switching frequency. Thus, the proceeding results are restricted to a frequency range sufficiently low such that the averaging approximation holds. During one period T, the system has state (20) for time DT for $k = 1, ..., M$ and state $U^{(\text{all grounded})} = 0$ for the remaining time:

$$U^{(avg)} = \frac{DT \times \sum_{k=1}^{k=M} U^{(k)}}{T} = \frac{V_{IN}}{N^2} \begin{bmatrix} M\mathcal{R}_C + \mathcal{R}_L \\ M\mathcal{R}_C + \mathcal{R}_L \\ \vdots \\ M\mathcal{R}_C + \mathcal{R}_L \\ 0 \end{bmatrix} D. \tag{21}$$

We define a matrix B as:

$$B \coloneqq \frac{V_{IN}}{N^2} \begin{bmatrix} M\mathcal{R}_C + \mathcal{R}_L \\ M\mathcal{R}_C + \mathcal{R}_L \\ \vdots \\ M\mathcal{R}_C + \mathcal{R}_L \\ 0 \end{bmatrix}, \tag{22}$$

where we assume V_{IN} is constant and treat the duty cycle D as an input. We can now write the full state space model in the standard form $\dot{\mathbf{x}} = A\mathbf{x} + BD$ with the averaged matrices A and B.

Because the A matrix (19) is constant regardless of the switch configuration, it is independent of duty cycle in the averaged model. This arises because the state variables see the same passive network regardless of switch positions. This is an advantageous property since the internal system dynamics, such as passive phase current balancing, can be taken as independent of the duty cycle.

A steady state solution for $\dot{\mathbf{x}} = 0$ can be written as $\mathbf{x_{ss}} = -A^{-1}BD$ if A^{-1} exists. If all the parameters $R_w, \mathcal{R}_C, \mathcal{R}_L, N, C, R_o$ are finite, positive values (as is the case in a practical circuit), A may be inverted. However, if $R_w = 0$, A is singular and a unique solution does not exist. This is expected, as the winding resistance is the element that restricts the phase currents to a single solution. For example, for an $M = 4$ phase system, the steady state solution is:

$$\mathbf{x_{ss}} = \begin{bmatrix} i_1 \\ i_2 \\ i_3 \\ i_4 \\ v_o \end{bmatrix} = -A^{-1}BD = \begin{bmatrix} \frac{1}{R_w+4R_o} \\ \frac{1}{R_w+4R_o} \\ \frac{1}{R_w+4R_o} \\ \frac{1}{R_w+4R_o} \\ \frac{4R_o}{R_w+4R_o} \end{bmatrix} DV_{IN}. \tag{23}$$

This reveals that current sharing is inherently guaranteed in a symmetric multiphase coupled inductor buck converter if the winding resistances are well matched.

B. Transfer Function of the M-phase Converter

The duty ratio to output voltage transfer function of a state space model in standard form is $G(s) = C(sI - A)^{-1}B$. Here, C is the output matrix. To study the duty cycle to output voltage characteristics, let $C = [0, 0, ..., 1]$.

The inverse $(sI - A)^{-1}$ is cumbersome to compute for an unknown M, but the problem is simplified if we assume that all phase currents are equal. If the structure is symmetric, all phases have the same reluctance $\mathcal{R}_L$ and winding resistance R_w, so the currents will be equal in state space averaging. Moreover, each phase has the same dynamic equation and is affected identically by the duty cycle input. It may be shown, by leveraging the symmetry of A, that the same transfer function can be found without assuming equal phase currents. However, the assumption significantly simplifies the derivation. So, we assert that

$$i_1 = i_2 = \cdots = i_M, \tag{24}$$

$$i_T = i_1 + i_2 + \cdots + i_M = Mi_1. \tag{25}$$

Then, we rewrite equation (16) in terms of total current i_T:

$$\begin{aligned} N^2 \frac{di_T}{dt} = Mv_o(-\mathcal{R}_L - M\mathcal{R}_C) + i_T[-R_w(\mathcal{R}_L + M\mathcal{R}_C)] \\ + MV_{IN}(\mathcal{R}_L + \mathcal{R}_C). \end{aligned} \tag{26}$$

We follow the same averaging procedure on (26) over a switching period and combine the dynamic equations into a reduced order state space model (27) with only two states: the total current i_T and the output voltage v_o:

$$\begin{aligned} \begin{bmatrix} \dot{i_T} \\ \dot{v_o} \end{bmatrix} &= \overbrace{\frac{1}{N^2}\begin{bmatrix} -R_w(M\mathcal{R}_C + \mathcal{R}_L) & -M(M\mathcal{R}_C + \mathcal{R}_L) \\ N^2\frac{1}{C} & -N^2\frac{1}{R_oC} \end{bmatrix}}^{A'} \begin{bmatrix} i_T \\ v_o \end{bmatrix} \\ &\quad + \underbrace{\frac{V_{IN}}{N^2}\begin{bmatrix} M(M\mathcal{R}_C + \mathcal{R}_L) \\ 0 \end{bmatrix}}_{B'} D, \qquad C' = \begin{bmatrix} 0 & 1 \end{bmatrix}. \end{aligned} \tag{27}$$

The reduced order system has fixed size regardless of M, so the transfer function may be computed easily. Since we seek the small signal transfer function, we write (27) in terms of perturbations of output voltage and duty cycle, $\tilde{v_o}$ and $\tilde{d}$:

$$\begin{aligned} G(s) &= \frac{\tilde{v_o}}{\tilde{d}}(s) = C'(sI - A')^{-1}B' \\ &= \frac{MV_{IN}R_o}{CL_{ptr}R_os^2 + (L_{ptr} + CR_wR_o)s + (MR_o + R_w)}. \end{aligned} \tag{28}$$

Here $L_{ptr} = L_l = \frac{N^2}{\mathcal{R}_L + M\mathcal{R}_C}$. (28) is a second order system regardless of the number of phases, due to the symmetry assumption. It is identical to a single-phase buck transfer function. The system bandwidth of (28) is:

$$\omega_o = \sqrt{\frac{(\mathcal{R}_L + M\mathcal{R}_C)(MR_o + R_w)}{N^2CR_o}} = \sqrt{\frac{MR_o + R_w}{L_{ptr}CR_o}}. \tag{29}$$

We write the bandwidth in terms of reluctances and inductances, where the first form is useful for physical design. Assuming $M\mathcal{R}_C \gg \mathcal{R}_L$ and $MR_o \gg R_w$, which is the case for many converters depending on load, number of phases, and reluctances, the bandwidth is approximately:

$$\omega_o \approx \sqrt{\frac{(M\mathcal{R}_C)(MR_o)}{N^2CR_o}} = \frac{M}{N}\sqrt{\frac{\mathcal{R}_C}{C}}. \tag{30}$$

That is, the bandwidth is primarily determined by the center leg reluctance.

In summary, $L_{ptr} = L_l = \frac{N^2}{\mathcal{R}_L + M\mathcal{R}_C}$ is a critical design parameter for the multiphase coupled inductor buck converter. It describes the per-phase transient inductance of the coupled inductor and is closely related to the output current ripple in steady-state through L_{oss} and the interleaving factor $1/\delta$. It equals the leakage inductance L_l in the multiwinding transformer model. If $\mathcal{R}_C \gg \mathcal{R}_L$, L_{ptr} is dominated by $\mathcal{R}_C$. It also determines the small signal transfer function of the multiphase buck converter in state-space-averaging. The control to output transfer function of a M-phase N-turn buck converter with a coupled inductor whose center leg reluctance is $\mathcal{R}_C$ and side leg reluctance is $\mathcal{R}_L$, is equivalent to the control to output transfer function of a M-phase uncoupled buck converter with a per-phase inductance $L_l = \frac{N^2}{\mathcal{R}_L + M\mathcal{R}_C}$.

C. Transfer Function Based on Circuit Models

The same insights on control to output transfer function can also be obtained from Fig. 3 or Fig. 4 to build circuit intuition. The analysis assumes that the duty cycles for each phase are identical, and thus the average voltages at nodes v_1 to v_M in Fig. 3 or Fig. 4 are identical to those input terminals to the coupled inductor are effectively shorted together. Thus, all the windings are effectively connected in parallel, with all input terminals connected together and all the output terminals connected together. We consider the response to a perturbation to the nominal operating point. With a symmetric model and identical voltages applied across the windings, the perturbation currents in all the windings will be identical.

The ideal current equalizing transformer in Fig. 3 (in blue) must also have equal current in each winding. Thus, one possible solution is all the winding current flowing through the ideal transformer, and no current in the magnetizing branches. Consideration of the voltage relationship shows that it is the unique, correct solution. If some of the winding current flowed through the magnetizing branches, the magnetizing current in each would need to be identical, both by symmetry and as enforced by the ideal current equalizing transformer. Producing these equal currents through the magnetizing branch impedance would require equal voltages across each. The voltages must sum to zero, so the only valid solution is zero voltage across and thus zero current through each magnetizing branch. The voltages at the nodes between the current equalizing transformer and the leakage inductors are all equal to the input voltage. Thus, all M leakage inductors are effectively in parallel, and the averaged control model is identical to that of a single-phase buck converter with an inductor value L_l/M. The magnetizing inductance L_μ has no impact on the dynamic response.

A similar argument applies to Fig. 4: With equal current perturbations due to symmetry, the current in the $\{M - 1\}$ turn winding of each ideal transformer balances the current in the other M windings, leaving zero current in the magnetizing inductance. Thus, all transformer winding voltages are zero. The voltages at the nodes between the current equalizing transformer and the leakage inductors (L_l) are all equal to the

TABLE I
DESIGN PARAMETERS OF THE PROTOTYPE COUPLED INDUCTOR

Measured	L_S	13.62 μH	L_{otr}	574 nH
Extracted	$\mathcal{R}_L$	1,091,625 H^{-1}	$\mathcal{R}_C$	1,166,888 H^{-1}
Calculated	$\mathcal{R}_L^*$	920,693 H^{-1}	$\mathcal{R}_C^*$	1,512,460 H^{-1}
Resistance	R_w	70.25 mΩ	R_o	1.5 Ω
Inductance Dual	L_L	1.09 μH	L_C	662 nH
Multiwind. Xformer	L_l	2.30 μH	L_μ	11.3 μH
Inductance Matrix	L_S	13.62 μH	L_M	-3.77 μH
Steady-state	L_{oss}	4.02 μH	L_{pss}	8.96 μH
Transient	L_{otr}	574 nH	L_{ptr}	2.30 μH
$\mathcal{FOM} = L_{ptr}/L_{pss}$	25.6%, 4x reduction in per-phase current ripple			

input voltage, the leakage inductors are effectively in parallel, and the averaged control model is identical to that of a single-phase buck converter with an inductor value L_l/M.

V. EXPERIMENTAL VERIFICATION

To verify and demonstrate the effectiveness of the inductance dual model, a multiphase inductor with programmable coupling coefficient was designed and fabricated. Fig. 6 shows a picture of the prototype, the 3D structure, and finite element modeling of the four-phase coupled inductor. Consider a typical four phase coupled inductor buck converter where fast transient response and low current ripple are needed. Equation (11) shows that L_{pss} can be increased by reducing center leg reluctance $\mathcal{R}_C$ (to reduce current ripple) and L_{otr} can be decreased by increasing $\mathcal{R}_C$ (to improve transient performance). This is a fundamental challenge in buck converter design: higher inductance yields smaller steady state ripple, while lower inductance results in faster transient response time. A programmable design that can switch between high and low $\mathcal{R}_C$ is attractive, such as the one suggested in [23]: a conductor passes a dc current through the center leg, saturating part of it and increasing the center leg reluctance to modulate the transient and steady state performance of the coupled inductor.

A four phase coupled core was designed using a finite element modeling tool (ANSYS Maxwell). An auxiliary current through the center leg is simulated to verify the reluctance programming behavior. Table I lists the designed and measured reluctance values. The coupled inductor is included in a 1 MHz four phase coupled inductor buck converter with 12 V input voltage, 1.5 V output voltage. Its power rating is 30 W. The maximum output current is 20 A. Fig. 7 shows the measured current waveforms of the multiphase buck converter with a four-phase coupled inductor without programming the core. The core is made of Ferroxcube 3F4.

Fig. 8 shows the theoretical frequency response of the converter by using the inductance dual model. A higher $\mathcal{R}_C$ leads to smaller L_{ptr} and thus pushes the control bandwidth to higher frequencies. Fig. 9 shows the measured duty ratio to output voltage frequency response. The bandwidth of the system is increased from about 16.1 kHz to 20.1 kHz with a 4 A auxiliary current in the center leg. Note that the approximate bandwidth expression (30) predicts a bandwidth of 18.5 kHz for the system. Based on the bandwidth increase, $\mathcal{R}_C$ has increased to around 2.4×10^6 H^{-1} with the auxiliary current of 4 A.

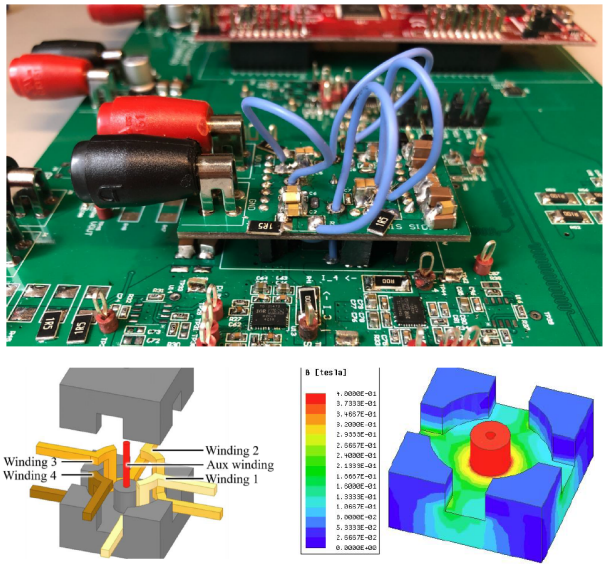

Fig. 6. (a) Picture of the prototype four-phase coupled inductor buck converter with programmable center leg reluctance. The coupled inductor is between the top and bottom PCBs.(b) ANSYS Maxwell model showing two halves of magnetic core (gray), four windings (gold), and auxiliary winding (red). (c) Partial center leg saturation with 1 A auxiliary current in ANSYS simulation.

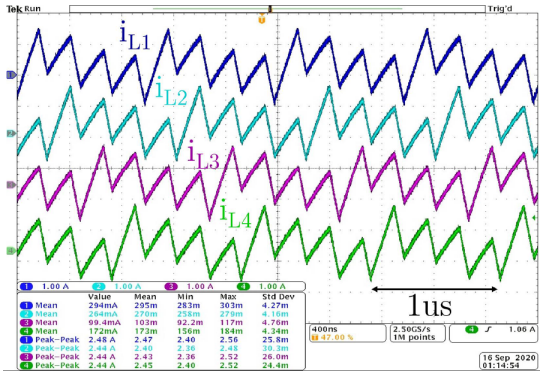

Fig. 7. Measured current waveforms of the 1 MHz, 8 V-1.5 V four-phase coupled inductor buck converter. A non-programmable core is used in this experiment, with different parameters from Table I.

The experimental setup described in this paper is not a practical programmable coupled inductor system, because the bandwidth only changes 25% for a substantial auxiliary current. One factor which diminishes the change in bandwidth is the fringing fields, which are not affected by the auxiliary current. However, we do achieve the desired behavior of changing the bandwidth, although the effect is smaller than expected. Further experiments with different center leg radii will be conducted that may improve the system programmability. If a significant bandwidth change is achieved, an example application of the circuit would be turning on the auxiliary current and increasing the control bandwidth when high load variation is expected, e.g., in microprocessor voltage regulators.

VI. CONCLUSIONS

This paper presents an inductance dual model for the design and simulation of multiphase coupled inductor buck converters. The inductance dual model links the physical magnetic

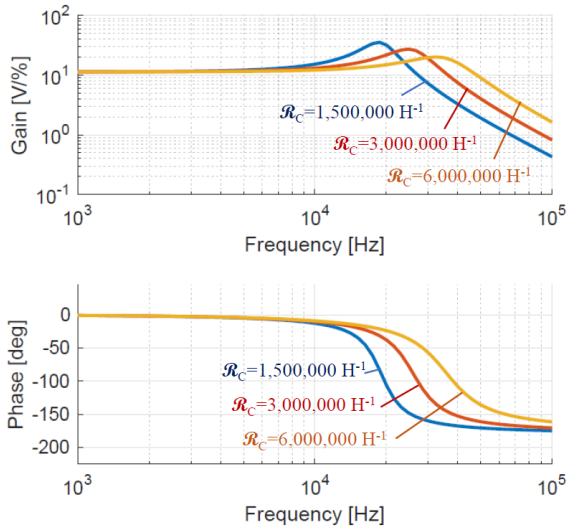

Fig. 8. Theoretical duty ratio to output voltage frequency response of four-phase coupled inductor from derivation in section IV-B. The bandwidth is increased for increasing center leg reluctance.

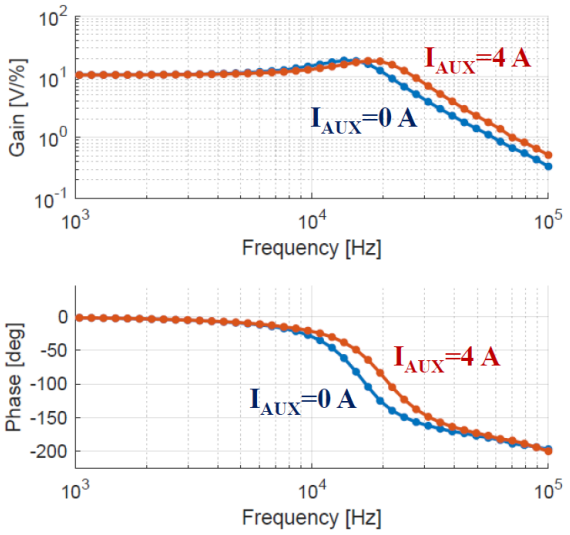

Fig. 9. Measured duty ratio to output voltage frequency response of four-phase coupled inductor buck with and without 4 A auxiliary winding current. The bandwidth, taken at $-90°$ phase, is increased from 16.1 kHz to 20.1 kHz with the auxiliary current on and center leg saturated.

structure to electrical behavior of the magnetic components in circuits. In SPICE, the model is suitable for visualization of multiphase coupling interactions. A set of equations are derived for predicting the effective inductance and current ripple. These equations are functionally identical to existing models but offer additional insight for physical design. The inductance dual model is used to derive the state space model and transfer function of a multiphase coupled inductor buck converter with an arbitrary number of phases in a symmetric magnetic structure. The transfer function is shown to be identical to an M-phase uncoupled buck or a single phase buck with appropriate inductances. The effectiveness of the inductance model is demonstrated by designing a programmable inductor for improved transient response.

VII. Acknowledgements

This work was jointly supported by the DOE ARPA-E DIFFERENTIATE program, the National Science Foundation (Award #1847365) .

References

[1] X. Zhou, P.-L. Wong, P. Xu, F. C. Lee, and A. Q. Huang, "Investigation of candidate VRM topologies for future microprocessors," *IEEE Trans. Power Electron.*, vol. 15, Nov. 2000.

[2] MIT EE Staff, *Magnetic Circuits and Transformers*, Cambridge MA: The MIT Press, 1943.

[3] P.-L. Wong, P. Xu, P. Yang, and F.C. Lee, "Performance Improvements of Interleaving VRMs with Coupling Inductors," *IEEE Trans. on Power Electronics*, vol. 16, no. 4, pp. 499–507, 2001.

[4] J. Li, C. R. Sullivan, A. Schultz, "Coupled Inductor Design Optimization for Fast-response Low-Voltage DC-DC Converters," *IEEE Applied Power Electronics Conference and Exposition*, APEC 2002, pp. 817–823 vol.2.

[5] J. Li, A. Stratakos, C. R. Sullivan, A. Schultz, "Using Coupled Inductors to Enhance Transient Performance of Multi-Phase Buck Converters," *IEEE Applied Power Electronics Conference and Exposition*, APEC 2004, pp. 1289–1293 vol.2.

[6] A. V. Ledenev, G. G. Gurov, and R. M. Porter, "Multiple Power Converter System Using Combining Transformers", US Patent US 6,545,450 B1, April 8, 2003.

[7] P. Zumel, O. Garcia, J. A. Cobos, J. Uceda, "Magnetic integration for interleaved converters", *Applied Power Electronics Conference*, 2003, APEC03.

[8] Y. Dong, "Investigation of Multiphase Coupled-Inductor Buck Converters in Point-of-Load Applications", *PhD Thesis*, Virginia Tech, Blacksburg, VA, Mar., 2009.

[9] A. M. Schultz and C. R. Sullivan, "Voltage converter with coupled inductive windings, and associated methods," U.S. Patent 6,362,986, March 26, 2002.

[10] D. C. Hamill, "Lumped equivalent circuits of magnetic components: the gyrator-capacitor approach," *IEEE Transactions on Power Electronics*, vol. 8, no. 2, pp. 97-103, April 1993.

[11] R. D. Middlebrook and S. Cuk, "A general unified approach to modelling switching-converter power stages," *1976 IEEE Power Electronics Specialists Conference*, Cleveland, OH, 1976, pp. 18-34.

[12] G. Zhu and K. Wang, "Modeling and design considerations of coupled inductor converters," *IEEE Applied Power Electronics Conference and Exposition (APEC)*, 2010.

[13] G. Zhu, B. A. McDonald and K. Wang, "Modeling and Analysis of Coupled Inductors in Power Converters," *IEEE Transactions on Power Electronics*, vol. 26, no. 5, pp. 1355-1363, May 2011.

[14] D. C. Prince, "Rectifier voltage control," *Journal of the A.I.E.E.*, vol. 45, no. 7, pp. 630-636, July 1926.

[15] S. El-Hamamsy and E. I. Chang, "Magnetics modeling for computer-aided design of power electronics circuits," *IEEE Power Electronics Specialists Conference*, Milwaukee, WI, USA, 1989, pp. 635-645 vol.2.

[16] E. C. Cherry, "The duality between interlinked electric and magnetic circuits and the formation of transformer equivalent circuits," *Proceedings of the Physical Society*, vol. 62 part 2, section B, no. 350 B, Feb. 1949, pp. 101-111.

[17] W. H. Hayt and J. E. Kemmerly, "Inductance and Capacitance: Duality," in *Engineering Circuit Analysis*, Fourth Edition, New York: McGraw-Hill Book Company, 1993.

[18] C. P. Steinmetz, "On the law of hysteresis AIEE Transactions", *Proceedings of the IEEE*, vol. 9, no. 2, pp. 3-64, 1892.

[19] J. Li, T. Abdallah, and C.R. Sullivan, "Improved calculation of core loss with non-sinusoidal waveforms", *Proc. IEEE IAS 2001*, pp. 2203-2210.

[20] J. Mühlethaler, J. Biela, J. W. Kolar and A. Ecklebe, "Improved core-Loss calculation for magnetic components employed in power electronic Systems," *IEEE Trans. on Power Electron.*, vol. 27, no. 2, pp. 964-973, Feb. 2012.

[21] B. Miwa, "Interleaved Conversion Techniques for High Density Power Supplies," *PhD Thesis*, Massachusetts Institute of Technology, 1992.

[22] C. Chang and M. A. Knights, "Interleaving technique in distributed power conversion systems," *IEEE Transactions on Circuits and Systems I: Fundamental Theory and Applications*, vol. 42, no. 5, pp. 245-251, May 1995.

[23] P. Zacharias, T. Kleeb, F. Fenske, J. Wende and J. Pfeiffer, "Controlled magnetic devices in power electronic applications," *2017 19th European Conference on Power Electronics and Applications* (EPE'17 ECCE Europe), Warsaw, 2017, pp. P.1-P.10.